



HAL
open science

Structure-Based Design and Synthesis of Piperidinol-Containing Molecules as New Mycobacterium abscessus Inhibitors

Jérôme Ruyck, Christian Dupont, Elodie Lamy, Vincent Le Moigne,
Christophe Biot, Yann Guerardel, Jean-louis Herrmann, Mickael Blaise,
Stanislas Grassin-delyle, Laurent Kremer, et al.

► **To cite this version:**

Jérôme Ruyck, Christian Dupont, Elodie Lamy, Vincent Le Moigne, Christophe Biot, et al.. Structure-Based Design and Synthesis of Piperidinol-Containing Molecules as New Mycobacterium abscessus Inhibitors. ChemistryOpen, 2020, 9 (3), pp.351-365. 10.1002/open.202000042 . hal-02988322

HAL Id: hal-02988322

<https://hal.science/hal-02988322>

Submitted on 5 Nov 2020

HAL is a multi-disciplinary open access archive for the deposit and dissemination of scientific research documents, whether they are published or not. The documents may come from teaching and research institutions in France or abroad, or from public or private research centers.

L'archive ouverte pluridisciplinaire **HAL**, est destinée au dépôt et à la diffusion de documents scientifiques de niveau recherche, publiés ou non, émanant des établissements d'enseignement et de recherche français ou étrangers, des laboratoires publics ou privés.

Structure-Based Design and Synthesis of Piperidinol-Containing Molecules as New *Mycobacterium abscessus* Inhibitors

Jérôme de Ruyck,^[a] Christian Dupont,^[b] Elodie Lamy,^[c] Vincent Le Moigne,^[c] Christophe Biot,^[a] Yann Guérardel,^[a] Jean-Louis Herrmann,^[c, d] Mickaël Blaise,^[b] Stanislas Grassin-Delyle,^[c, e] Laurent Kremer,^[b, f] and Faustine Dubar^{*[a]}

Non-tuberculous mycobacterium (NTM) infections, such as those caused by *Mycobacterium abscessus*, are increasing globally. Due to their intrinsic drug resistance, *M. abscessus* pulmonary infections are often difficult to cure using standard chemotherapy. We previously demonstrated that a piperidinol derivative, named PIPD1, is an efficient molecule both against *M. abscessus* and *Mycobacterium tuberculosis*, the agent of tuberculosis, by targeting the mycolic acid transporter MmpL3. These results prompted us to design and synthesize a series of

piperidinol derivatives and to determine the biological activity against *M. abscessus*. Structure-activity relationship (SAR) studies pointed toward specific sites on the scaffold that can tolerate slight modifications. Overall, these results identified FMD-88 as a new promising active analogue against *M. abscessus*. Also, we determined the pharmacokinetics properties of PIPD1 and showed that intraperitoneal administration of this compound resulted in promising serum concentration and an elimination half-life of 3.2 hours.

1. Introduction

Non-tuberculous mycobacteria (NTM) are environmental bacterial isolated from surface and tap water, soil, animals, milk and food products.^[1,2] They are responsible for opportunistic infections in humans and are recognized as an increasing public health concern. NTM have been reported as a cause of diverse

infectious diseases in humans, livestock, and wildlife, such as pulmonary, extra-pulmonary, skin and soft tissue infections.^[3]

The diseases caused by NTM are increasing on a worldwide scale.^[4] In developed countries, NTM lung infections are more prevalent than TB.^[5-7] Nearly 200 distinct NTM species have been reported so far, with the *Mycobacterium avium-intracellulare* complex (MAC) and the *Mycobacterium abscessus* as the major causative agents in Europe as well as in the United States.^[8,9] Of particular concern, *M. abscessus* infects both immunocompromised or immunocompetent individuals and is often associated with cystic fibrosis (CF).^[10-12] In CF patients, presence of *M. abscessus* in the lungs correlates with a decline in the lung function and can be fatal.^[13-15] In addition, recent studies suggested a transmission of *M. abscessus* complex between CF patients^[10,16,17], although this transmission might be indirect, through fomites and dust.^[18]

The current standardized antimicrobial treatment for *M. abscessus* infections^[10] combines three drugs, or more, for at least 12 months. Moreover it is aggressive and burdensome.^[12] The outcome of the treatment is also highly dependent on the inducible resistance to macrolides^[19,20] (clarithromycin or azithromycin), leading to a treatment success rate below 40%.^[21] Lung transplantation in CF patients, often representing the last therapeutic option, is currently being debated amongst clinicians in the case of pre-existing infection with *M. abscessus*. However, most centers do not consider the presence of *M. abscessus* as an absolute contra-indication since recent studies support the possibility of lung transplantation with favorable outcome in CF patients.^[12,14,20,22-24] In light of the limited panel of available drugs active against *M. abscessus*, treatments are often complex and challenging. In this context, it appears necessary to identify efficient, specific and less toxic compounds.

[a] Dr. J. de Ruyck, Prof. C. Biot, Dr. Y. Guérardel, Dr. F. Dubar
Univ. Lille, CNRS
UMR 8576 – UGSF – Unité de Glycobiologie Structurale et Fonctionnelle
59000 Lille (France)
E-mail: faustine.dubar@univ-lille.fr

[b] Dr. C. Dupont, Dr. M. Blaise, Dr. L. Kremer
IRIM Institut de Recherche en Infectiologie de Montpellier – UMR9004-CNRS/
UM
1919 route de Mende
34293 Montpellier (France)

[c] E. Lamy, Dr. V. Le Moigne, Prof. J.-L. Herrmann, Dr. S. Grassin-Delyle
Infection et inflammation – Laboratoire 2I
UMD1173-INSERM/UVSQ
Versailles, 2 Avenue de la source de la Bièèvres
78180 Montigny le Bretonneux (France)

[d] Prof. J.-L. Herrmann
Université Paris-Saclay, UVSQ, INSERM, Infection et Inflammation
(U1173), Montigny le Bretonneux, France

[e] Dr. S. Grassin-Delyle
Hôpital Foch
Département des maladies des voies respiratoires
92150 Suresnes (France)

[f] Dr. L. Kremer
INSERM, Institut de Recherche en Infectiologie de Montpellier, Montpellier,
France

Supporting information for this article is available on the WWW under
<https://doi.org/10.1002/open.202000042>

© 2020 The Authors. Published by Wiley-VCH Verlag GmbH & Co. KGaA. This is an open access article under the terms of the Creative Commons Attribution Non-Commercial NoDerivs License, which permits use and distribution in any medium, provided the original work is properly cited, the use is non-commercial and no modifications or adaptations are made.

The lack of therapeutic solutions prompted us to perform a phenotypic screen for bactericidal compounds against *M. abscessus* using a library^[25] of compounds formerly validated for their activity against *M. tuberculosis*.^[26] Our study allowed identifying a new piperidinol-based compound, which we named PIPD1 (Figure 1) and which exhibits potent activity against clinical isolates of *M. abscessus in vitro* and in infected human macrophages and zebrafish embryos.^[26]

Importantly, *M. abscessus*-infected zebrafish embryos treated with PIPD1 showed an increased survival rate and a decrease in bacterial burden, as compared to the infected but non-treated animals. Thanks to the selection of spontaneous resistant mutants and following whole-genome sequencing, single nucleotide polymorphisms (SNP) were identified in *MAB_4508*. This gene encodes the mycolic acid transporter MmpL3 that was shown to be essential for *Mycobacterium smegmatis* and *M. tuberculosis* survival.^[27–29] Like other MmpL, MmpL3 is a transmembrane protein belonging to the Resistance-Nodulation-Cell division (RND) permeases.^[30] MmpL proteins are known to participate in the export of lipid components across the cell envelope in mycobacteria. We demonstrated that PIPD1 does not affect *de novo* biosynthesis of mycolic acid but rather inhibits the transport of trehalose monomycolate (TMM) by blocking the flippase activity of MmpL3.^[26,31] This results in the loss of trehalose dimycolate synthesis, the decrease of arabinogalactan mycolylation and bacterial death. Herein, with the aim to improve the activity of this new family of MmpL3 inhibitors against *M. abscessus*, we present the rational design and the structure-activity relationships of piperidinol derivatives.

2. Results and Discussion

2.1. Chemistry

In the present study, a first series of piperidinol-based compounds with potent antibacterial activity against *M. abscessus* was synthesized. The initial hit compound, PIPD1, was derived in order to identify the pharmacophores and to explore a preliminary structure-activity relationship (SAR). The new derivatives were evaluated against the *M. abscessus* CIP104536^T reference strain. In addition, toxicity of the most potent compounds was evaluated in order to determine the selectivity

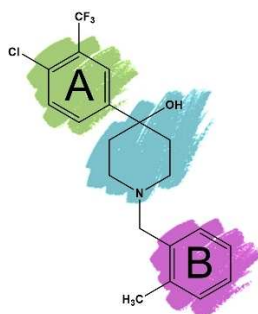


Figure 1. Chemical structure of PIPD1.

index. Moreover, all analogues were subjected to molecular modeling studies using MmpL3 in order to rationalize, at a molecular level, the *in vitro* results. Previously, PIPD1 was synthesized according to a reported method.^[26]

However, the synthetic method used (Figure 2) includes a deprotection step (Figure 2, step b), which is not complete and causes a degradation of the product of interest. Another deprotection condition using trifluoroacetic acid (TFA) was therefore evaluated, but degradation of the final product was still observed and the yield obtained for step b was insufficient to pursue the complete synthesis. In order to circumvent these limitations, another synthetic pathway was developed, as outlined in Figure 3.

First, *N*-benzylation was achieved by means of benzyl bromide in DCM in the presence of an excess of potassium carbonate, resulting in high yields of the piperidone product. Total consumption of the starting aldehyde was monitored by thin layer chromatography (TLC) using dichloromethane as eluent. Second, bromine–lithium exchange reaction was followed by a nucleophilic substitution reaction on the carbonyl of piperidinone to form the final compound. The final products were purified on silica gel chromatography. ¹H-NMR, ¹³C-NMR and mass spectrometry were performed to confirm the synthesized compound structures. Synthesis of all presented analogues was between 30–60% yield. Thus, this new synthetic route with limited reaction steps is associated to a significant improvement in the total yields of the analogues.

2.2. Biology and Structure Activity Relationship Study (SAR)

We first aimed at designing PIPD1 analogues to identify common pharmacophores in the first series of compounds

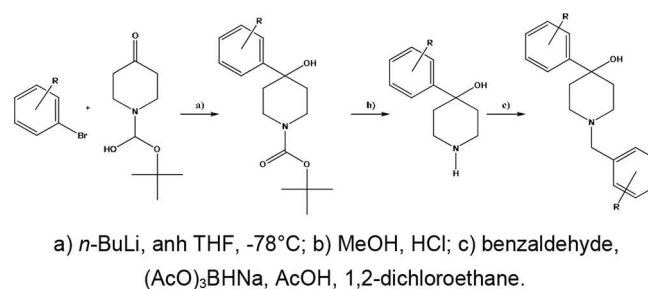


Figure 2. Three-step chemical synthesis of PIPD1 and related analogues.

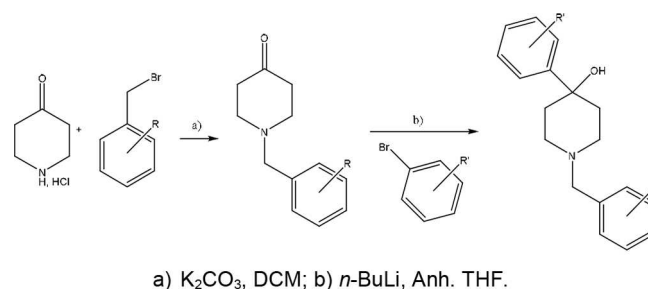


Figure 3. Two-step chemical synthesis of PIPD1 analogues.

(Series I). Among these compounds, each organic function, (designated A and B, see Figure 1) of PIPD1 were removed or modulated and the *in vitro* antimycobacterial activity of products against the *M. abscessus* smooth (S) reference strain CIP104536⁷ was assayed to attest for their contribution to the activity. The minimal inhibitory concentration (MIC) expressed in $\mu\text{g/ml}$ (and $\mu\text{mol/L}$) was determined using Cation-adjusted Mueller-Hinton (CaMHb; Sigma-Aldrich), according to CLSI guidelines.^[32] The evaluation of the toxicity of the newly synthesized compounds was evaluated on mammalian cells in order to establish a selectivity index. Toxicity assays on Vero cells were performed in RPMI supplemented with 10% FBS based on cell viability using resazurin as a cell survival indicator. The half maximal inhibitory concentration (IC_{50}) corresponds to the drug concentration that reduces cell viability by 50% and is expressed in percentage of cell survival.

The selectivity index (SI_{Mabs}), corresponding to the $\text{IC}_{50}/\text{MIC}$ ratio was determined for the 12 most active compounds against *M. abscessus*. IC_{50} and SI were not determined for compounds with unsatisfactory biological activity ($\text{MIC}_{99} > 0.5 \mu\text{g/ml}$). Table 1 summarizes the structures and inhibition activities of the designed PIPD1-analogues of the series I.

Results in Table 1 indicate that the aromatic parts A and B and the tertiary alcohol function of the piperidinol moiety are essential for the inhibitory activity against *M. abscessus*. Moreover, the methyl group of the ring B participates to the antimycobacterial effect since the activity of FMD-15 was lower than the one of PIPD1. The donor inductive effect of methyl group may impact the inhibitory effect. With respect to ring A, the removal of the trifluoromethyl group (FMD-32) clearly impacted on the biological activity as compared to the removal of the chlorine atom (FMD-33).

Although the dataset of compounds tested is limited, important SAR elements have been unravelled and subsequently utilized for guiding the design of the series II compounds (Table 2).

From these data, one can deduce that the aromatic moieties are key to the biological activity. The nature of the aromatic substituent was modulated to determine if steric effect influences the activity. The steric occupancy of the aromatic ring A appeared significant, nevertheless the lack of the trifluoromethyl and methyl groups on naphthalene could explain the decrease of activity for naphthalene (FMD-102). The steric hindrance was also an important feature in ring B since the introduction of a bulky substituent (such as ferrocene in FMD-6 or an aromatic-substituted piperidine in FMD-62) caused a decrease in bactericidal activity against *M. abscessus*. Additionally, the modification of the methyl group of ring B was investigated in relation to their position and electronic properties. The presence of a substituent in ring B with a consistent steric hindrance appears essential to biological activity. Indeed, PIPD1 with a methyl substituent and FMD-88 with an iodo substituent were more active than FMD-3 that carries a fluorine atom. Additionally, the position of the substituents on ring B also appears important since the presence of group in the *ortho* position (PIP1, FMD-88 or FMD-93) initiates a potent antimycobacterial activity, whilst the presence of methyl group at

Table 1. Structures and biological evaluation (MIC_{99} , CC_{50} and SI; N.D., not determined) of the PIPD1-derivatives of the series I. MIC_{99} (*M. abscessus*) data result from three independent experiments and CC_{50} (Vero cells) from two independent experiments.

Analogues	Formula	MIC_{99} <i>M.abs</i> [$\mu\text{g}/\text{ml}$]	MIC_{99} <i>M.abs</i> [$\mu\text{mol}/\text{L}$]	CC_{50} [$\mu\text{g}/\text{ml}$]	SI_{Mabs}
PIP1		0.125	0.3	25	200
FMD-37		128	350.6	N.D.	N.D.
FMD-16		128	623.9	N.D.	N.D.
FMD-32		2	6.3	N.D.	N.D.
FMD-33		1	2.9	N.D.	N.D.
FMD-15		1	2.7	N.D.	N.D.
FMD-99		4	14.2	N.D.	N.D.
FMD-0		128	458.7	N.D.	N.D.
FMD-46		64	261.1	N.D.	N.D.

meta (FMD-63) or *para* (FMD-66) positions decreases the activity. Noteworthy, these results are similar to those reported against *M. tuberculosis*,^[31] which strongly suggests that the mechanism of inhibition and/or binding site of these compounds in MmpL3 are conserved in *M. tuberculosis* and *M. abscessus*. To further rationalize these experimental data, the synthesized derivatives were subjected to *in silico* docking analyses using a 3D homology model of MmpL3 from *M. abscessus* to address how the different SAR elements interact with MmpL3 at a molecular level.

Table 2. Structures and biological evaluations (MIC_{99} , CC_{50} and SI; N.D., not determined) of the series II PIPD1-analogues. MIC_{99} (*M. abscessus*) data are from three independent experiments and CC_{50} (Vero cells) are from two independent experiments.

Analogues	Formula	MIC_{99} <i>M. abs</i> [$\mu\text{g/ml}$]	MIC_{99} <i>M. abs</i> [$\mu\text{mol/L}$]	CC_{50} [$\mu\text{g/ml}$]	SI_{Mabs}
FMD-88		0.125	0.25	25	200
FMD-93		0.125	0.3	50	400
FMD-96		0.125	0.3	25	200
FMD-89		0.125	0.3	50	400
PIPD-1		0.125	0.3	25	200
FMD-91		0.25	0.6	25	100
FMD-10		0.25	0.7	50	200
FMD-94		0.5	1.1	50	100
FMD-3		1	2.6	N.D.	N.D.
FMD-61		2	4.8	N.D.	N.D.
FMD-63		2	5.2	N.D.	N.D.
FMD-66		2	5.2	N.D.	N.D.
FMD-6		4	8.4	N.D.	N.D.
FMD-103		4	9.6	50	12.5
FMD-9		4	9.7	N.D.	N.D.

Table 2. continued

Analogues	Formula	MIC_{99} <i>M. abs</i> [$\mu\text{g/ml}$]	MIC_{99} <i>M. abs</i> [$\mu\text{mol/L}$]	CC_{50} [$\mu\text{g/ml}$]	SI_{Mabs}
FMD-92		4	9.9	N.D.	N.D.
FMD-102		4	12.1	N.D.	N.D.
FMD-64		16	36.6	N.D.	N.D.
FMD-62		32	70.8	N.D.	N.D.

2.3. Molecular Modelling

Previously, several mutations in *M. abscessus* strains resistant to PIPD1 were identified in *MAB_4508*, that encodes the TMM transporter MmpL3.^[26,31] Moreover, we recently demonstrated that PIPD1 alters the mycolic acid transport in *M. abscessus*^[26] by directly inhibiting the TMM flippase activity of MmpL3 in *M. tuberculosis*.^[31] Finally, Zhang et al. solved the crystal structure of *Mycobacterium smegmatis* MmpL3 by X-ray crystallography at a resolution of 2.8 Å (PDB:6AJJ) which unravelled a cavity in the transmembrane region of MmpL3 accommodating several MmpL3 inhibitors.^[33] Since MmpL3 and its orthologues are well conserved across mycobacteria, comparative modelling of *M. abscessus* MmpL3 using the crystal structure of *M. smegmatis* MmpL3 as a template (sharing 65% identity with its *M. abscessus* orthologue) was performed (Figure 4a and 4b). Quality of the *M. abscessus* MmpL3 model was then evaluated according to classical geometric parameters (See SI for full report). The RMSD calculated on the C_{α} of the template is around 0.4 Å and 96% of the residues are within the Ramachandran criteria. The superimposition of the *M. abscessus* MmpL3 model onto the *M. smegmatis* MmpL3 structure showed that the drug binding site formerly described^[33] was conserved in the transmembrane domain of the *M. abscessus* MmpL3 (gold sphere in Figure 4). Interestingly, this cavity is in the vicinity of residues previously reported to participate to the proton relay.^[26,31,33] This binding pocket is composed of two hydrophobic cavities, designated Up- and Bottom-pockets (U and B in Figure 4c) and comprises also a more polar cavity, designated Middle-pocket (M in Figure 4c). Of note, the residues contouring the M- and B-pockets are well conserved amongst all mycobacteria (see sequence alignment Figure S1).

Docking simulations and energy minimization were next conducted using the *M. abscessus* MmpL3 predictive model with different analogues: the reference compound PIPD1, one analogue with a higher inhibitory effect (FMD-89), one with a lower inhibitory effect (FMD-61), one truncated ligand (FMD-0).

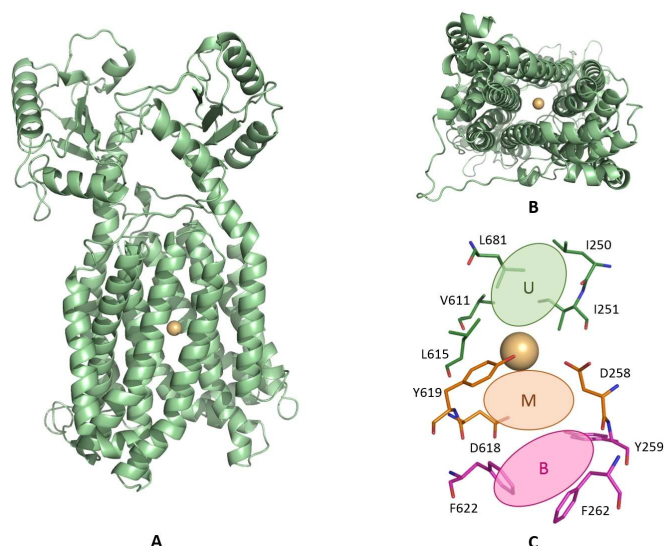


Figure 4. A) Comparative model of *M. abscessus* MmpL3 lacking its C-terminal region. The binding pocket (Gold Sphere) is located inside the transmembrane channel. B) 90° rotation of Figure 5A clearly showing the channel. C) Focus on the putative binding site surrounded by three regions, two hydrophobic pockets (U and B) and a more polar pocket (M).

In order to consider protonated or unprotonated states of piperidinol tertiary amine at physiological pH, docking simulations were performed on both structures for each compound. Results were similar after the two runs and, thus, only unprotonated ligands are presented in this article.

After minimization of the simulated PIPD1 complex, the best binding pose was retrieved and further analysed (Figure 5A and 5B). On one side, PIPD1 is hydrogen-bound to the carboxylic acid group of D618 through its amino moiety. On the other side, its hydroxyl group is H-bound to the hydroxyl of Y219. Additionally, a potent interaction with the carboxylic acid group of D258 can occur. Thanks to these two strong interactions, the ligand appears perfectly anchored into the proposed proton channel of the transporter. Additional stabilization occurred through π - π interactions between the toluene moiety of PIPD1 and phenyl rings of F262 and F622 (B-pocket). However, the U-pocket does not appear to be optimally filled.

Regarding FMD-89, due to the electron-releasing effect of the chloride moiety grafted on the phenyl ring, the π - π interactions with the phenyl rings of F262 and F622 are increased, which likely explains the change in antimicrobial properties (Figure 5C). Chlorobenzyl group perfectly fits the B-pocket while the central core of the compound is well stabilized by the hydrogen bonds. The presence of a second *ortho* chlorine substitution on ring B (FMD-94) causes a decrease in the biological activity, as compared to FMD-89 (Table 2). This could be explained by a reduction of π - π stacking interactions with the phenyl rings of F262 and F622 (Figure 5D) since the aromatic ring B is no longer in a favourable position, due to the presence of the chlorine atom in the two *ortho* positions of ring B. These results demonstrate that the additional chloride group alters the binding in the B-pocket inducing a change in conformation of the central core.

We next simulated a lower affinity complex by studying the replacement of the chlorobenzene ring of FMD-89 with a naphthalene group in FMD-61 (Figure 5E and 5F), which was designed to keep the aromatic property of the substitution as compared to PIPD1. In Figure 5E, the nitrogen atom is located towards the U-pocket and the hydroxyl located towards the B-pocket. In addition, no more residues are involved in hydrogen bonds. As expected, the ligand is now located upside-down (Figure 5F) in the binding pocket, as compared to PIPD1. This drastic change in conformation could explain the loss of antimicrobial activity due to absence of the two key interactions (H-bonds) between the PIPD1 hydroxyl group and Y219 and between the PIPD1 ammonium group and D258, as illustrated in Figure 5B. Indeed, neither the hydrogen bonds nor the π - π interactions are observed. Only small hydrophobic or van der Waals interactions can explain these binding modes. It can therefore be speculated that the B-pocket is too narrow, therefore only accommodating small aromatic moieties.

Finally, the truncated ligand FMD-0 is obviously not well adapted to the binding site. Nevertheless, this last binding pose (Figure 5G) clearly explains why the hydroxyl group of the central ring of any inhibitors is required. Here, only the important hydrogen bond between D258 and the hydroxyl moiety is conserved. Moreover, the lack of interaction in the B-pocket seems to induce large changes in the conformation of the putative inhibitors. These poor interactions may contribute to the low antimicrobial properties of the inhibitor.

Furthermore, the nature of the *ortho* group in ring B appears important too. Even though the electronic effects do not have a significant influence to the binding capacity of the PIPD1 analogues, the size of the substituents, however, seems to have a great impact to their biological activity. Indeed, the methyl group (2.00 Å) in PIPD1 or the iodine atom (1.98 Å) in FMD-89 are associated with a more pronounced activity than the fluorine atom (1.47 Å) in FMD-3. To get insights into these differences, the steric hindrance of the *ortho* substituent for FMD-89 and FMD-3 within the binding site of MmpL3 were modelled (Figure 6).

As shown in Figure 6A the iodine atom of FMD-89 is blocked in the binding cavity of the active site and allows to increase the capability of the aromatic group to be stabilized by π - π interactions (Figure 6B). In contrast, the ring B ring of FMD-3 adopts a slightly different orientation than the B ring of FMD-89 due to smaller size of the fluorine atom. These observations confirm that FMD-3 displays a weaker interaction than FMD-89, particularly for the π - π stacking of ring B.

2.4. Toxicology and Pharmacokinetics Studies

To evaluate the preclinical pharmacokinetic profiles of PIPD1, survival curves were assessed for 96 h in BALB/c mice, following intraperitoneal (IP) injection with increasing concentrations of PIPD1, ranging from 10 mg/kg to 250 mg/kg. Whereas IP administration of the higher dose led to rapid death after 48 h, injection of 100 mg/kg was associated with a 67% survival rate and administration of 50 mg/kg led to 100% survival after 96 h

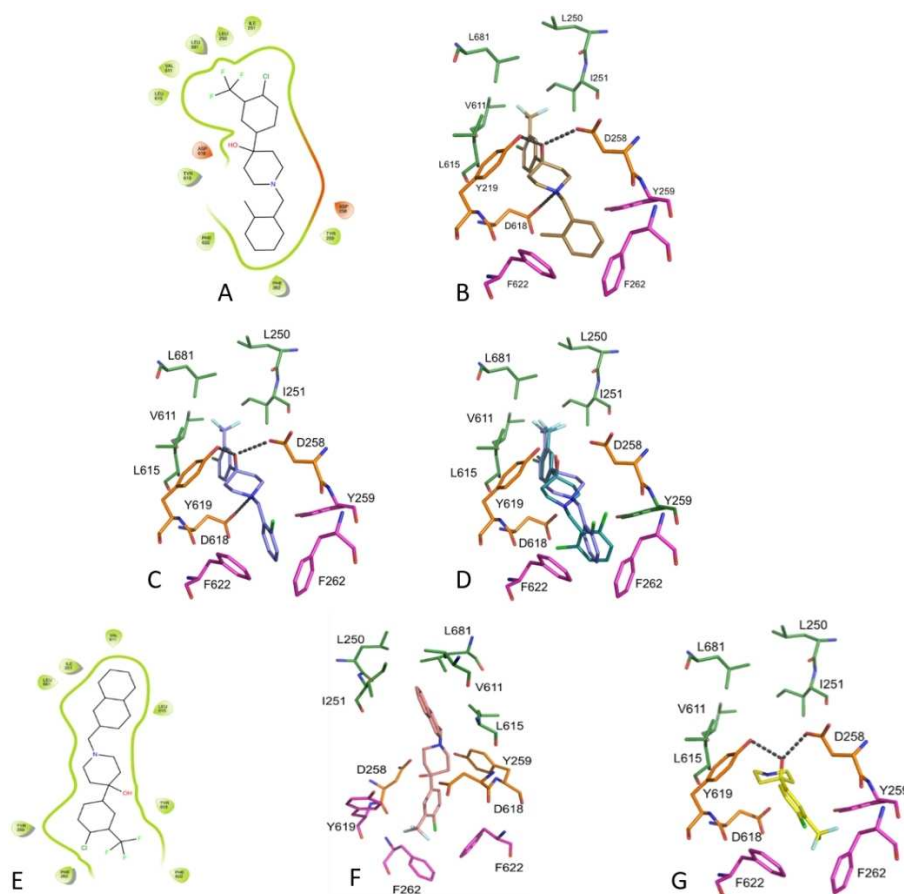


Figure 5. A) Interaction diagram of PIPD1 in the binding pocket of MmpL3. Residues contouring the active site are represented in green while H-bonded residues to ligands are highlighted in red. B) Molecular representation of the interaction of PIPD1 and MmpL3 pocket. C) Binding mode of the FMD-89 compound. D) Comparison of FMD-89 (purple sticks) and FMD-94 (turquoise sticks). E) Interaction diagram of FMD-61 in the binding pocket of MmpL3. F) Molecular representation of FMD-61 and MmpL3 pocket. G) Binding mode of the truncated derivative (FMD-0).

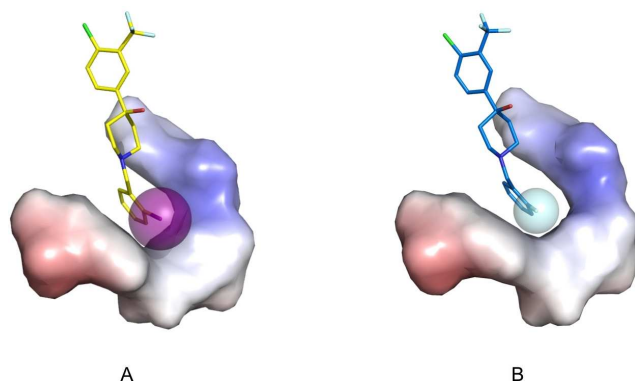


Figure 6. Steric hindrance of *ortho* substituent in ring B for FMD-89 (A) and FMD-3 (B). Spheres radii are directly proportional to the Van der Waals radii of each atom.

post-injection. According to these results, a dose of 50 mg/kg was used as the working concentration for all subsequent pharmacokinetics studies after IP administration or oral gavage. The concentration vs time profiles in the serum and tissues are shown in Figure 7.

Following IP injection, the serum concentration was measured at 600 ng/mL after 5 min and the drug distribution was found to be greater in the lungs, the kidney, the spleen and the heart, as compared to the brain and the liver. The concentrations obtained after IP administration were 6.9 mL/min for clearance, 1.9 L for the central volume of distribution, 4.9 mL/min for inter-compartmental clearance and 2.0 L for the peripheral volume of distribution. The elimination half-life was about 3.2 h. On the other hand, serum concentrations after oral administration remained below 100 ng/mL and the relative oral bioavailability of the compound was estimated to be lower than 10% (when compared to the IP route). Since PIPD1 is a lipophilic compound ($\log P=4.9$), the digestive absorption is expected to be important and the low oral bioavailability rather suggests a strong hepatic first-pass effect, although other mechanisms such as efflux by active transporters (P-glycoprotein or multidrug resistance proteins) cannot be excluded at this stage. The hypothesis of hepatic first-pass effect is reinforced by the observation of a second peak in serum concentration occurring after 8 h, suggesting the existence of an entero-hepatic cycle. PIPD1 exhibited a good organ distribution after IP administration and was rapidly eliminated with a half-life of about 3 h.

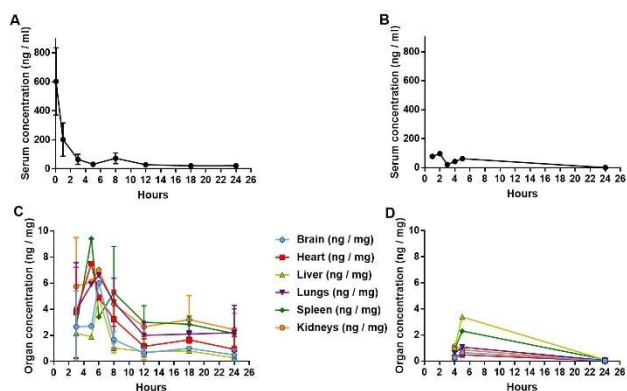


Figure 7. Pharmacokinetic analysis of PIPD1 in female BALB/c mice after intraperitoneal injection (A, C) or oral gavage (B, D). (A) Concentration in sera and (C) concentration in organs following a single 50 mg/kg dose administered using the IP route. (B) Concentration in sera and (D) concentration in organs following a single 50 mg/kg dose administered orally.

3. Conclusions

In the present report, SAR studies emphasize the contribution of the two aromatic moieties (ring A and ring B) as well as the importance of the steric hindrance of the substituent on ring B. Based on molecular modeling studies, we propose that the size of ring B in the binding cavity is limited and could explain poor biological activity of the PIPD1-analogues comprising a large group. Nevertheless, the stability of the analogues/MmpL3 complexes is enhanced when the ring B is totally blocked in the active site. Moreover, we demonstrated that PIPD1 exhibits a good organ distribution after IP administration in mice and was rapidly eliminated with a half-life of about 3 h. Drugs with short half-life that are totally cleared within a few hours only are usually easier to manipulate, especially if they present toxicity issues. With respect to oral administration, the low relative bioavailability could be explained either by a poor intestinal absorption or a strong metabolic clearance. Thus, investigation of these processes for the newly synthesized analogues is warranted by the advantages and ease of oral administration in patients. In a forthcoming work PIPD1 will be modified in order to increase polarity and to minimize phase I metabolism, based on the PK study. Altogether, these results pave the way for the development of a new generation of anti-MmpL3 inhibitors with improved activity against *M. abscessus*.

Experimental Section

Chemistry

Nuclear magnetic resonance (^1H , ^{13}C , and ^{19}F NMR) spectra were recorded at room temperature on a Bruker AC 300 spectrometer. TMS was used as an internal standard and CDCl_3 as the solvent. ^1H NMR analyses were obtained at 300 MHz (s: singlet, br s: broad singlet, d: doublet, t: triplet, dd: double doublet, td: double triplet); ^{13}C NMR analyses were obtained at 75.4 MHz; and ^{19}F NMR analyses were obtained at 282 MHz. The chemical shifts (δ) are given in parts

per million relative to TMS ($\delta=0.00$). Mass spectra were recorded by means of a Waters Micromass Quattro II triple quadrupole LC mass spectrometer equipped with electrospray ionization (ESI) and atmospheric pressure chemical ionization (APCI) sources. Column chromatography, carried out on silica gel (Merck Kieselgel 60) was used for the purification of compound. Reactions were monitored by thin-layer chromatography (TLC) coated silica gel plates and detection by UV lamp. The purity degree of compound was checked by NMR and MS analysis and proved to be higher than 95%.

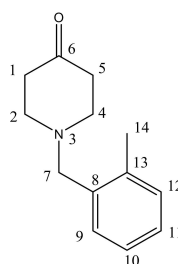
All chemicals reagents were purchased at Sigma-Aldrich. Dry THF was obtained from a solvent purification system (Innovative Technology Inc. MA, USA, Pure-Solv)

General Procedure for the Synthesis of PIPD1-Derivatives

First step: 4-Piperidinone monohydrate hydrochloride (1 g, 6.5 mmol) is suspended in dichloromethane (DCM, 120 ml, 1.9 mol) and methanol (4 ml, 0.09 mol). Then K_2CO_3 (2 g, 0.01 mol) is added. The mixture is stirred during 30 min then of α -Bromo-O-xylene (0.86 ml, 6.5 mmol) is added. The mixture is stirred during 12 h at room temperature. The mixture is quenched with distilled water (100 ml, 5.5 mol) then the aqueous layer is extracted by DCM (2×100 ml, 3.2 mol). The organic layer is dried on Na_2SO_4 before filtration. Solvents are removed under reduce pressure. The residue is purified on flash chromatography (silica gel) with a gradient eluent (DCM: 100 to DCM/MeOH: 95/5)..

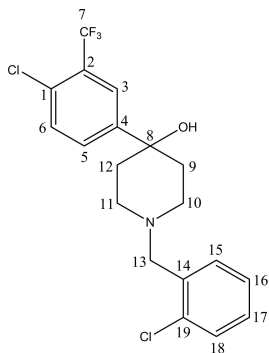
Second step: Under N_2 , bromine derivative (1 eq) is dissolved in anhydrous THF (5 ml, 0.06 mol for 1 eq of bromine derivative). The solution is cooled at -78°C before the slow addition of n-Butyl Lithium solution (2.5 M in hexane; 1 eq). The mixture is stirred during 1 h at -78°C . Under N_2 , the compound obtained in the first step is dissolved in anhydrous THF (5 ml, 0.06 mol for 1 eq of bromine derivative), then the reaction is stirred during 2 h at -78°C . The reaction is quenched by saturated solution of NH_4Cl (at -78°C) then the mixture is abandoned at room temperature before adding of distilled water (50 ml, 2.8 mol). The mixture is extracted by ethyle acetate (3×50 ml, 1.5 mol). The organic layer is dried on Na_2SO_4 before filtration. Solvents are removed under reduce pressure. The residue is purified on flash chromatography (silica gel) with a gradient eluent (DCM: 100 to DCM/MeOH: 95/5).

1-(2-methylbenzyl)piperidin-4-one



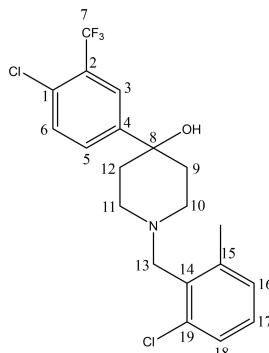
^1H NMR (300 MHz, CDCl_3) δ 7.18 (dd, $J=9.5, 7.8$ Hz, 4H, H9, H10, H11 and H12), 3.68 (m, 2H, H7), 2.92 (m, 2H, H2 and H4), 2.68 (m, 4H, H1 and H5), 2.67 (m, 2H, H2 and H4), 2.37 (m, 3H, H14). ^{13}C NMR (75 MHz, CDCl_3) δ 205.7 (C6), 138.1 (C8), 136.5 (C13), 130.3 (C12), 128.1 (C9), 126.6 (C10), 125.3 (C11), 61.6 (C7), 51.0 (C2 and C4), 39.7 (C1 and C5), 19.4 (C14). $M/Z=203.13$ g/mol. Colorless oil. Yield = 95%

FMD-88



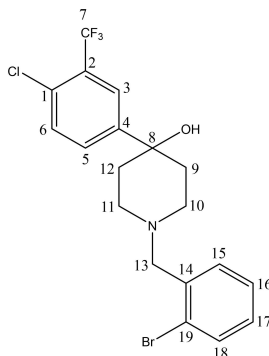
^1H NMR (300 MHz, CDCl_3) δ 7.84(s, 1H, H18), 7.80 (d, $J=9.0$ Hz, 1H, H3), 7.58 (d, $J=8.3$ Hz, 1H, H6), 7.42 (d, $J=8.3$ Hz, 2H, H5 et H16), 7.31 (t, $J=7.2$ Hz, 1H, H17), 6.94 (t, $J=7.3$ Hz, 1H, H15), 3.59 (s, 2H, H13), 2.81 (d, $J=10.6$ Hz, 2H, H10 and H11), 2.58 (t, $J=11.5$ Hz, 2H, H10 and H11), 2.13 (d, $J=2.8$ Hz, 2H, H9 and H12), 1.69 (d, $J=13.4$ Hz, 2H, H9 and H12). ^{13}C NMR (75 MHz, CDCl_3) δ 147.9 (C14), 140.6 (C19), 139.6 (C5), 131.3 (C15), 130.6 (C1), 130.4 (C6), 129.4 (C17), 128.8 (C18), 128.1 (C3), 124.9(C2), 124.2 (q, C16), 121.2 (C4), 100.8 (C7), 71.1 (C8), 66.6 (C13), 49.1 (C10 and C11), 38.5 (C9 and C12). M/Z = 495.01 g/mol. Yellow oil. Yield = 35 %

FMD-96



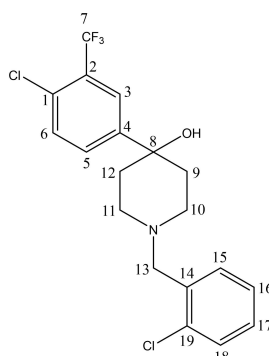
^1H NMR (300 MHz, CDCl_3) δ 7.83 (s, 1H, H18), 7.79 (d, $J=9.0$ Hz, 1H, H3), 7.60 (d, $J=8.3$ Hz, 1H, H6), 7.44 (d, $J=8.3$ Hz, 2H, H5 et H16), 7.21 (t, $J=7.2$ Hz, 1H, H17), 7.10 (t, $J=7.3$ Hz, 1H, H15), 3.72 (s, 2H, H13), 2.75 (d, $J=10.6$ Hz, 2H, H10 and H11), 2.61 (t, $J=11.5$ Hz, 2H, H10 and H11), 2.48 (s, 3H, CH_3), 2.03 (d, $J=2.8$ Hz, 2H, H9 and H12), 1.70 (d, $J=13.4$ Hz, 2H, H9 and H12). ^{13}C NMR (75 MHz, CDCl_3) δ 147.8 (C14), 141.0 (C19), 135.7 (C5), 134.32 (C15), 131.28 (C1), 129.35 (C6), 129.1 (C17), 128.1 (C18), 127.1 (C3), 124.8 (C2), 124.2 (q, C16), 121.2 (C4), 71.2 (C7), 56.3 (C8), 48.9 (C13), 38.7 (C10 and C11), 20.0 (CH_3). M/Z = 417.87 g/mol. Brown oil. Yield = 62 %

FMD-93



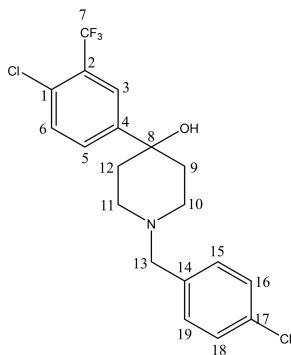
^1H NMR (300 MHz, CDCl_3) δ 7.87 (s, 1H, H18), 7.83 (d, $J=9.0$ Hz, 1H, H3), 7.59 (d, $J=8.3$ Hz, 1H, H6), 7.52 (d, $J=8.3$ Hz, 2H, H5 et H16), 7.28 (t, $J=7.2$ Hz, 1H, H17), 7.10 (t, $J=7.3$ Hz, 1H, H15), 3.59 (s, 2H, H13), 2.81 (d, $J=10.6$ Hz, 2H, H10 and H11), 2.58 (t, $J=11.5$ Hz, 2H, H10 and H11), 2.13 (d, $J=2.8$ Hz, 2H, H9 and H12), 1.69 (d, $J=13.4$ Hz, 2H, H9 and H12). ^{13}C NMR (75 MHz, CDCl_3) δ 147.8 (C14), 137.6 (C19), 132.8 (C5), 131.3 (C15), 130.8 (C1), 130.7 (C6), 129.4 (C17), 128.5 (C18), 127.9 (C3), 127.3 (C2), 124.8 (q, C16), 124.2 (C4), 121.2 (C7), 71.1 (C8), 61.9 (C13), 49.2 (C10 and C11), 38.5 (C9 and C12). M/Z = 447.02 g/mol. Dark yellow oil. Yield = 72 %

FMD-89



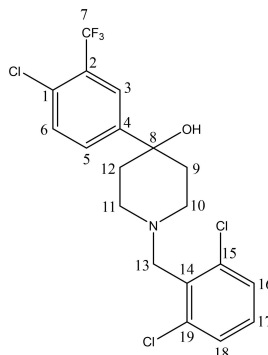
^1H NMR (300 MHz, CDCl_3) δ 7.86 (s, 1H, H18), 7.81 (d, $J=9.0$ Hz, 1H, H3), 7.60 (d, $J=8.3$ Hz, 1H, H6), 7.48 (d, $J=8.3$ Hz, 2H, H5 et H16), 7.34 (t, $J=7.2$ Hz, 1H, H17), 7.22 (t, $J=7.3$ Hz, 1H, H15), 3.69 (s, 2H, H13), 2.81 (d, $J=10.6$ Hz, 2H, H10 and H11), 2.53 (t, $J=11.5$ Hz, 2H, H10 and H11), 2.12 (d, $J=2.8$ Hz, 2H, H9 and H12), 1.67 (d, $J=13.4$ Hz, 2H, H9 and H12). ^{13}C NMR (75 MHz, CDCl_3) δ 147.9 (C14), 136.0 (C19), 131.4(C5), 130.8 (C15), 130.7 (C1), 129.6 (C6), 129.4 (C17), 128.3 (C18), 128.0 (C3), 126.7 (C2), 124.9 (q, C16), 124.3 (C4), 121.3 (C7), 71.1 (C8), 59.4 (C13), 49.3 (C10 and C11), 38.6 (C9 and C12). M/Z = 404.24 g/mol. Brown oil. Yield = 50 %

FMD-91



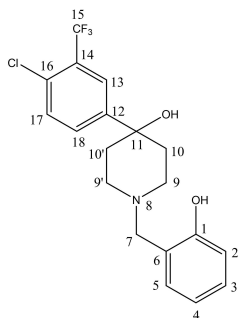
^1H NMR (300 MHz, CDCl_3) δ 7.84(s, 1H, H18), 7.80 (d, $J=9.0$ Hz, 1H, H3), 7.40 (d, $J=8.3$ Hz, 1H, H6), 7.58 (d, $J=8.3$ Hz, 2H, H5 et H16), 7.46 (t, $J=7.2$ Hz, 1H, H17), 7.28 (t, $J=7.3$ Hz, 1H, H15), 3.53 (s, 2H, H13), 2.75 (d, $J=10.6$ Hz, 2H, H10 and H11), 2.45 (t, $J=11.5$ Hz, 2H, H10 and H11), 2.10 (d, $J=2.8$ Hz, 2H, H9 and H12), 1.70 (d, $J=13.4$ Hz, 2H, H9 and H12). ^{13}C NMR (75 MHz, CDCl_3) δ 147.9 (C14), 136.6 (C19), 132.9 (C15), 131.3 (C1), 130.7 (C6), 130.5 (C17), 129.3 (C18), 128.4 (C3), 124.8 (C2), 124.1 (q, C16), 121.1 (C4), 100.8 (C7), 71.0 (C8), 62.27 (C13), 49.1 (C10 and C11), 38.4 (C9 and C12). $M/Z=404.24$ g/mol. Brown oil. Yield = 80%

FMD-94



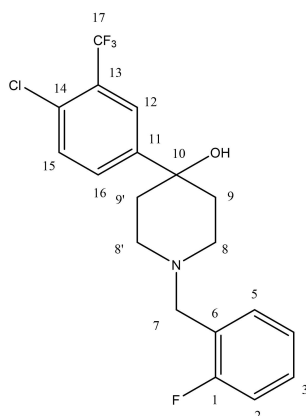
^1H NMR (300 MHz, CDCl_3) δ 7.84(s, 1H, H18), 7.58 (d, $J=9.0$ Hz, 1H, H3), 7.43 (d, $J=8.3$ Hz, 1H, H6), 7.30 (d, $J=8.3$ Hz, 2H, H5 et H16), 7.15 (t, $J=7.2$ Hz, 1H, H17), 3.82 (s, 2H, H13), 2.85 (d, $J=10.6$ Hz, 2H, H10 and H11), 2.68 (t, $J=11.5$ Hz, 2H, H10 and H11), 2.06 (d, $J=2.8$ Hz, 2H, H9 and H12), 1.70 (d, $J=13.4$ Hz, 2H, H9 and H12). ^{13}C NMR (75 MHz, CDCl_3) δ 147.8 (C14), 137.0 (C19), 134.5 (C15), 131.3 (C1), 130.6 (C6), 129.4 (C17), 128.9 (C18), 128.4 (C3), 128.3 (C2), 124.8 (q, C16), 124.1 (C4), 121.2 (C7), 71.1 (C8), 56.6 (C13), 49.1 (C10 and C11), 38.5 (C9 and C12). $M/Z=438.68$ g/mol. Brown oil. Yield = 32%

FMD10



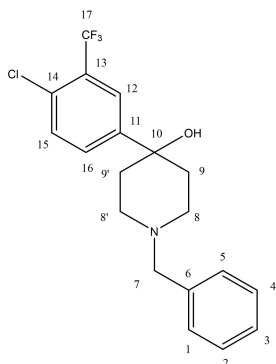
^1H NMR (300 MHz, CDCl_3) δ 7.84 (s, 1H, H13), 7.55 (d, $J=9$ Hz, 1H, H17), 7.46 (d, $J=9$ Hz, 1H, H18), 7.16 (t, $J=9$ Hz, 1H, H3), 6.98 (d, $J=9$ Hz, 1H, H5), 6.78 (d, $J=9$ Hz, 2H, H2 and H4), 3.75 (s, 2H, H7), 2.89 (d, $J=12$ Hz, 2H, H9 and H9'), 2.61 (t, $J=12$ Hz, 2H, H9 and H9'), 2.08 (t, $J=12$ Hz, 2H, H10 and H10'), 1.75 (d, $J=12$ Hz, 2H, H10 and H10'). ^{13}C NMR (75 MHz, CDCl_3) δ 157.69 (C^{IV} , C1), 147.26 (C^{IV} , C16), 131.53 (CH_{aromr} , C18), 131.08 (C^{IV} , C14), 128.91 (C^{IV} , C17), 124.78 (C^{IV} , C15), 124.22 (CH_{aromr} , C13), 121.26 (C^{IV} , C6), 119.43 (CH_{aromr} , C4), 116.08 (CH_{aromr} , C2), 70.69 (C^{IV} , C11), 61.51 (CH_2 , C7), 48.68 (2CH_2 , C9 and C9'), 38.24 (2CH_2 , C10 and C10'). $M/Z=385.11$ g/mol. Brown oil. Yield = 41%

FMD-3



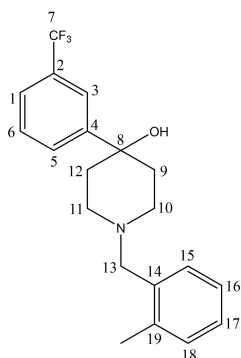
^1H NMR (300 MHz, CDCl_3) δ 7.86 (s, 1H, H12), 7.60 (d, $J=9.0$ Hz, 1H, H2), 7.43 (m, 2H, H3 et H15), 7.23 (m, 1H, H5), 7.08 (m, 2H, H4 et H16), 3.65 (s, 2H, H7), 2.81 (d, $J=9.0$ Hz, 2H, H8 et H8'), 2.52 (t, $J=12$ Hz, 2H, H8 et H8'), 2.14 (t, $J=9$ Hz, 2H, H9 et H9'), 1.68 (d, $J=12$ Hz, 2H, H9 et H9'). ^{13}C NMR (75 MHz, CDCl_3) δ 163.19 (C^{IV} , C1), 159.93 (C^{IV} , C14), 148.04 (C^{IV} , C13), 131.77 (CH_{aromr} , C3), 131.38 (CH_{aromr} , C15), 129.41 (C^{IV} , C11), 129.08 (CH_{aromr} , C2), 128.97 (CH_{aromr} , C5), 124.31 (C^{IV} , C6), 124.24 (C^{IV} , C4), 124.17 (C^{IV} , C12), 123.97 (C^{IV} , C17), 115.40 (CH_{aromr} , C16), 71.02 (C^{IV} , C10), 55.44 (CH_2 , C7), 48.99 (2CH_2 , C8 et C8'), 38.52 (2CH_2 , C9 et C9'). $M/Z=387.10$ g/mol. Brown oil. Yield = 44%

FMD-15



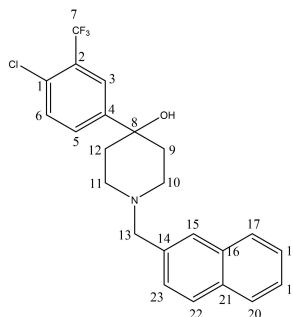
^1H NMR (300 MHz, CDCl_3) δ 7.86 (s, 1H, H12), 7.60 (d, $J=9.0$ Hz, 1H, H2), 7.45 (m, 2H, H3 et H15), 7.37–7.30 (m, 1H, H1 and H5), 7.21 (m, 2H, H4 et H5), 3.65 (s, 2H, H7), 2.81 (d, $J=9.0$ Hz, 2H, H8 et H8'), 2.52 (t, $J=12$ Hz, 2H, H8 et H8'), 2.14 (t, $J=9$ Hz, 2H, H9 et H9'), 1.68 (d, $J=12$ Hz, 2H, H9 et H9'). ^{13}C NMR (75 MHz, CDCl_3) δ 147.9 (C14), 139.6 (C5), 131.3 (C15 and C19), 130.6 (C1), 130.4 (C6), 129.4 (C17), 128.8 (C16 and C18), 128.1 (C3), 124.9(C2), 121.2 (C4), 100.8 (C7), 71.1 (C8), 66.6 (C13), 49.1 (C10 and C11), 38.5 (C9 and C12). $M/Z=369.11$ g/mol. Brown oil. Yield = 55 %

FMD-33



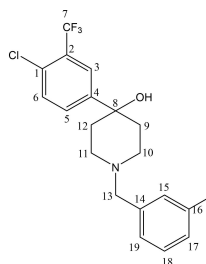
^1H NMR (300 MHz, CDCl_3) δ 7.56 (s, 1H, H3), 7.49 (s, 1H, H1), 7.32 (d, $J=33.1$ Hz, 1H, H5), 7.28–7.28 (m, 1H, H6), 7.20 (m, 1H, H16), 7.18 (dd, $J=9.3, 8.3$ Hz, 3H, H17, H18 and H19), 3.96 (s, 2H, H13), 2.68–2.63 (m, 2H, H11 and H10), 2.46 (m, 2H, H11 and H10), 2.36 (s, 3H, CH_3), 2.14 (m, 2H, H9 and H12), 1.87 (m, 2H, H9 and H12). ^{13}C NMR (75 MHz, CDCl_3) δ 139.9 (C4), 138.1 (C14), 136.5 (C19), 135.9 (C2), 130.3 (C18), 130.0 (C5), 129.9 (C6), 128.1 (C15), 126.6 (C16), 126.2 (C1), 125.3 (C17), 125.2 (C3), 124.1 (C7), 73.7 (C8), 61.6 (C13), 49.2 (C10 and C11), 37.5 (C9 and C12), 19.4 (CH_3). $M/Z=349.17$ g/mol. Black oil. Yield = 27 %

FMD-61



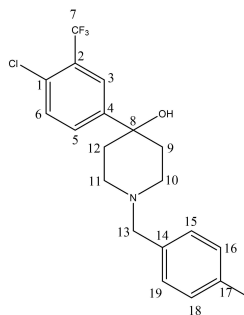
^1H NMR (300 MHz, CDCl_3) δ 7.77 (d, $J=18.5$ Hz, 1H, H17), 7.71 (s, 1H, H22), 7.61 (s, 1H, H3), 7.59 (s, 1H, H15), 7.44 (d, $J=18.5$ Hz, 1H, H15), 7.42 (m, 2H, H18 and H19), 7.28 (s, 1H, H6), 7.21 (d, $J=36.3$ Hz, 1H, H5), 3.63 (s, 2H, H13), 2.67 (m, 2H, H10 and H11), 2.49 (m, 2H, H10 and H11), 2.14 (m, 2H, H9 and H12), 1.87 (m, 2H, H9 and H12). ^{13}C NMR (75 MHz, CDCl_3) δ 139.1 (C4), 138.1 (C14), 136.1 (C2), 134.4 (C16), 134.2 (C1), 134.0 (C21), 131.3 (C5), 129.7 (C6), 128.9 (C17), 128.8 (C22), 128.8 (C15), 128.4 (C23), 128.3 (C20), 127.0 (C18), 125.6 (C19), 124.4 (C3), 124.0 (C7), 73.7 (C8), 64.2 (C13), 49.2 (C10 and C11), 37.5 (C9 and C12). $M/Z=419.30$ g/mol. Light brown oil. Yield = 19 %

FMD-63



^1H NMR (300 MHz, CDCl_3) δ 7.48 (s, 1H, H5), 7.28 (s, 1H, H6), 7.23 (m, 1H, H18), 7.20 (m, 1H, H5), 7.16 (m, 2H, H15 and H19), 7.09 (s, 1H, H17), 3.60 (s, 2H, H13), 2.67 (m, 2H, H10 and H11), 2.35 (s, 3H, CH_3), 2.32 (m, 2H, H10 and H11), 2.13 (m, 2H, H9 and H12), 1.93 (m, 2H, H9 and H12). ^{13}C NMR (75 MHz, CDCl_3) δ 139.1 (C14), 139.1 (C4), 138.4 (C16), 136.1 (C2), 134.2 (C1), 131.3 (C5), 129.7 (C6), 128.4 (C18), 127.7 (C15), 127.5 (C17), 125.9 (C19), 124.4 (C3), 124.0 (C7), 73.7 (C8), 64.0 (C4), 49.2 (C10 and C11), 37.5 (C9 and C12) 21.2 (CH_3). $M/Z=383.13$ g/mol. Brown oil. Yield = 49 %

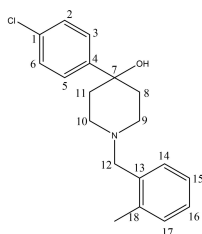
FMD-66



^1H NMR (300 MHz, CDCl_3) δ 7.48 (s, 1H, H3), 7.23 (dd, $J=25.6, 14.4$ Hz, 1H, H6), 7.22 (s, 1H, H5), 7.20 (m, 2H, H15 and H19), 7.16

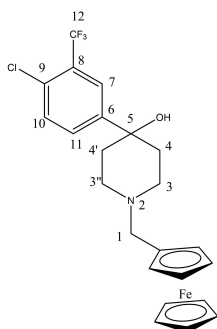
(m, 2H, H16 and H18), 3.56 (s, 2H, H13), 2.67 (m, 2H, H10 and H11), 2.34 (s, 3H, CH₃), 2.32 (m, 2H, H10 and H11), 2.13 (m, 2H, H9 and H12), 1.93 (m, 2H, H10 and H11). ¹³C NMR (75 MHz, CDCl₃) δ 139.1 (C1), 136.1 (C2), 135.2 (C17), 134.4 (C14), 134.2 (C1), 131.3 (C5), 129.8 (C16 and 18), 129.7 (C6), 129.5 (C15 and C19), 124.4 (C3), 124.0 (C7), 73.7 (C8), 63.7 (C13), 49.2 (C10 and C11) 37.5 (C9 and H12), 21.1 (CH₃). M/Z = 383.13 g/mol. Brown oil. Yield = 68%

FMD-32



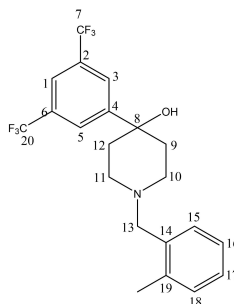
¹H NMR (300 MHz, CDCl₃) δ 7.30 (s, 1H, H6), 7.27 (s, 1H, H2), 7.18 (m, 2H, H3 and H5), 7.17 (s, 1H, H14), 7.15 (s, 1H, H17), 7.14 (s, 1H, H16), 7.13 (s, 1H, H15), 3.98 (s, 2H, H12), 2.65 (m, 2H, H9 and H10), 2.35 (m, 5H, H9, H10 and CH₃), 2.13 (m, 2H, H8 and H13), 1.93 (m, 2H, H8 and H13). ¹³C NMR (75 MHz, CDCl₃) δ 142.1 (C4), 138.1 (C13), 136.5 (C18), 136.2 (C1), 130.3 (C17), 129.4 (C2 and C6), 128.1 (C3 and C5), 128.1 (C3 and C5), 126.6 (C15), 125.3 (C16), 73.6 (C7), 61.6 (C12), 49.2 (C9 and C10), 37.5 (C8 and C11), 19.4 (CH₃). M/Z = 315.14 g/mol. Yellow oil. Yield = 57%

FMD-6



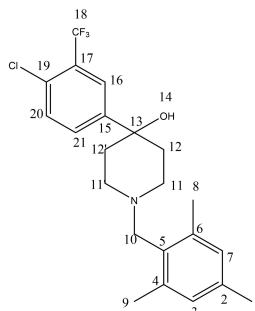
¹H NMR (300 MHz, CDCl₃) δ 7.83 (s, 1H, H7), 7.52 (d, J = 9 Hz, 1H, H10), 7.41 (d, J = 9 Hz, 1H, H11), 4.10 (s, 2H, Cp), 4.08 (s, 5H, Cp'), 4.06 (s, 2H, Cp), 3.38 (s, 2H, H1), 2.7 (d, J = 12 Hz, 2H, H3 et H3'), 2.39 (t, J = 12 Hz, 2H, H3 et H3'), 2.06 (t, J = 9 Hz, 2H, H4 et H4'), 1.59 (d, J = 9 Hz, 2H, H4 et H4'). ¹³C NMR (75 MHz, CDCl₃) δ 131.20 (CH_{aromr} C11), 130.36 (C^{IV}, C9), 129.36 (CH_{aromr} C10), 128.00 (C^{IV}, C8), 124.82 ((C^{IV}, C6), 124.23 (CH_{aromr} C7), 121.20 (C^{IV}, C12), 70.52 (C^{IV}, C5), 70.39 (2CH_{aromr} Cp), 68.54 (5CH_{aromr} Cp'), 68.18 (2CH_{aromr} Cp), 58.18 (CH₂, C1), 48.33 (2CH₂, C3 et C3'), 37.96 (2CH₂, C4 et C4'). M/Z = 477.08 g/mol. Yellow oil. Yield = 46%

FMD103



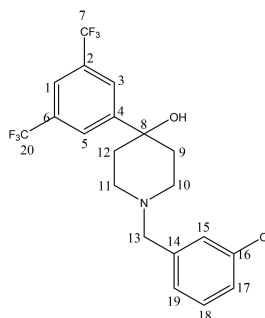
¹H NMR (300 MHz, CDCl₃) δ 7.80 (s, 1H, H1), 7.66 (m, 2H, H3 and H5), 7.20 (m, 1H, H15), 7.18 (dd, J = 10.5, 4.7 Hz, 1H, H18), 7.17 (m, 2H, H16 and H17), 3.72 (s, 2H, H13), 2.65 (m, 1H, H10 and H11), 2.45 (m, 2H, H10 and H11), 2.38 (s, 3H, CH₃), 2.15 (m, 2H, H9 and H12), 1.89 (m, 2H, H9 and H12). ¹³C NMR (125 MHz, CDCl₃) δ 143.0 (C4), 139.0 (C2 and C6), 138.1 (C14), 136.5 (19), 130.3 (C18), 128.6 (C3 and C5), 128.1 (C15), 126.6 (C16), 125.3 (C1 and 17), 124.4 (C7 and C20), 73.7 (C8), 61.6 (C13), 49.2 (C10 and C11), 37.5 (C9 and C12) 19.4 (CH₃). M/Z = 417.15 g/mol. Brown oil. Yield = 62%

FMD-9



¹H NMR (300 MHz, CDCl₃) δ 7.81 (s, 1H, H6), 7.52 (d, J = 9 Hz, 1H, H21), 7.40 (d, J = 9 Hz, 1H, H20), 6.83 (s, 2H, H3 and H7), 3.49 (s, 2H, H10), 2.71 (d, J = 9 Hz, 2H, H11 and H11'), 2.36 (d, J = 9 Hz, 6H, H8 and H9), 2.24 (d, J = 6 Hz, 3H, H1), 1.95 (d, J = 9 Hz, 2H, H12 and H12'), 1.61 (d, J = 9 Hz, 2H, H12 and H12'). ¹³C NMR (75 MHz, CDCl₃) δ 148.0 (C5), 137.4 (C2, C4 and C6), 136.5 (C19), 132.1 (C17), 132.1 (C21), 129.4 (C20), 129.1 (C3 and C7), 124.9 (C15), 124.2 (C16), 121.3 (C18), 71.4 (C13), 59.1 (C10), 48.93 (2CH₂, C11 and C11'), 38.85 (2CH₂, C12 and C12'), 20.97 (CH₃, C1), 20.17 (2CH₃, C8 and C9). M/Z = 411.16 g/mol. Brown oil. Yield = 28%

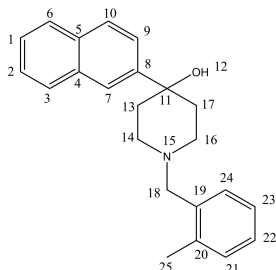
FMD-92



¹H NMR (300 MHz, CDCl₃) δ 7.74 (s, 1H, H1), 7.59 (m, 2H, H3 and H5), 7.32 (s, 1H, H15), 7.21 (t, J = 15.1 Hz, 3H, H17, H18 and H19), 3.67 (s,

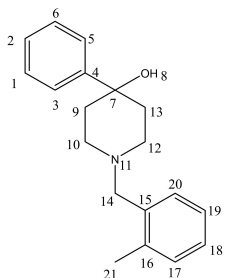
2H, H13), 2.64 (m, 2H, H10 and H11), 2.46 (m, 2H, H10 and H11), 2.15 (m, 2H, H9 and H12), 1.95 (m, 2H, H9 and H12). ^{13}C NMR (75 MHz, CDCl_3) δ 143.0 (C4), 141.2 (C14), 139.0 (C2 and C6), 133.3 (C16), 129.2 (C18), 128.6 (C15), 128.6 (C3 and C5), 127.1 (C19), 126.7 (C17), 125.3 (C1), 124.4 (C7 and C20), 73.67, 64.0 (C13), 49.2 (C10 and C11), 37.5 (C9 and C12). $M/Z=403.07$ g/mol. Dark yellow oil. Yield = 41 %

FMD-102



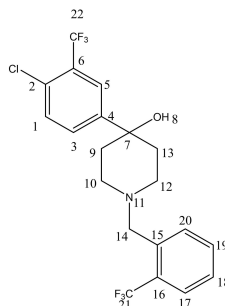
^1H NMR (300 MHz, CDCl_3) δ 7.82 (m, 1H, H3), 7.79 (m, 2H, H6 and H10), 7.78 (s, 1H, H7) 7.48–7.40 (m, 3H, H1, H2 and H9), 7.22–7.14 (m, 4H, H21, H22, H23 and H24), 3.64 (s, 2H, H18), 2.69 (m, 2H, H14 and H16), 2.44 (m, 2H; H14 and H16), 2.34 (s, 3H, H25), 2.16 (m, 2H, H13 and H17), 1.89 (m, 2H, H13 and H17). ^{13}C NMR (75 MHz, CDCl_3) δ 142.3 (C8), 138.1 (C19), 136.5 (C20), 134.5 (C5), 134.0 (C4), 130.3 (C21), 130.2 (C10), 129.7 (3), 128.2 (C6), 128.1 (C24), 127.0 (C1), 126.6 (C23 and C9), 126.5 (C2), 125.3 (C22), 123.4 (C7), 73.5 (C11), 61.6 (C18), 49.2 (C14 and C16), 37.5 (C13 and C17), 19.4 (C25). $M/Z=331.19$ g/mol. White oil. Yield = 71 %

FMD-99



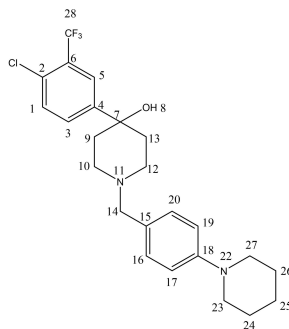
^1H NMR (300 MHz, CDCl_3) δ 7.29 (m, 2H, H1 and H6), 7.25 (m, 2H, H3 and H5), 7.21 (m, 2H, H2 and H20), 7.18 (m, 1H, H19), 7.17 (m, 1H, H18), 7.16 (m, 1H, H16), 3.67 (s, 2H, H14), 2.72 (m, 2H, H10 and H12), 2.50 (m, 2H, H10 and H12), 2.34 (s, 3H, H21), 2.18 (m, 2H, H9 and H13), 1.91 (m, 2H, H9 and H13). ^{13}C NMR (75 MHz, CDCl_3) δ 143.4 (C4), 138.1 (C15), 136.5 (C16), 130.3 (C17), 128.5 (C1 and C6), 128.2 (C2), 128.1 (C20) 126.6 (C19), 126.3 (C3 and C5), 125.3 (C18), 73.6 (C7), 61.6 (C14), 49.2 (C10 and C12), 37.5 (C9 and C13), 19.4 (C21). $M/Z=281.18$ g/mol. Colorless oil. Yield = 52 %

FMD-64



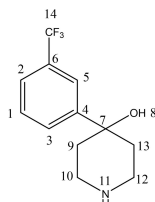
^1H NMR (300 MHz, CDCl_3) δ 7.56 (d, $J=1.5$ Hz, 2H, H5 and H17), 7.34 (s, 1H, H19), 7.30 (m, 1H, H1), 7.24 (m, 2H, H3 and H20), 7.21 (m, 1H, H18), 3.87 (s, 2H, H14), 2.78 (m, 2H, H10 and H12), 2.46 (m, 2H, H10 and H12), 2.18 (m, 2H, H9 and H13), 1.91 (m, 2H, H9 and H13). ^{13}C NMR (75 MHz, CDCl_3) δ 139.1 (C4), 136.1 (C6), 134.7 (C15), 134.2 (C2), 132.0 (C19), 131.3 (C3), 129.9 (C20), 129.7 (C1), 128.0 (C16), 126.7 (C18), 126.6 (C17), 125.0 (C22), 124.4 (C5), 124.0 (C26), 73.7 (C7), 61.7 (C14), 49.2 (C10 and C12) 37.5 (C9 and C13). $M/Z=437.10$ g/mol. Yellow oil. Yield = 34 %

FMD-62



^1H NMR (300 MHz, CDCl_3) δ 7.55 (s, 1H, H5), 7.30 (s, 1H, H1), 7.21 (s, 1H, H3), 7.05 (m, 2H, H16 and H20), 6.68 (m, 2H, H17 and H19), 3.44 (s, 2H, H14), 3.41 (m, 2H, H23 and H27), 3.14 (m, 2H, H23 and H27), 2.65 (m, 2H, H10 and H12), 2.42 (m, 2H, H10 and H12), 2.13 (m, 2H, H9 and H13), 1.90 (m, 2H, H9 and H13), 1.68 (m, 4, H24 and H26), 1.62 (m, 2H, H25). ^{13}C NMR (75 MHz, CDCl_3) δ 148.7 (C18), 139.1 (C4), 136.1 (C6), 134.2 (C2), 131.3 (C3), 129.7 (C1), 129.4 (C16 and C20), 128.6 (C15), 124.4 (C5), 124.0 (C28), 114.1 (C17 and C19), 73.7 (C7), 63.7 (C14), 49.7 (C23 and C27), 49.2 (C10 and C12), 37.5 (C9 and C13), 25.1 (C24 and C26), 23.4 (C25). $M/Z=452.18$ g/mol. Brown oil. Yield = 41 %

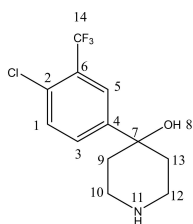
FMD46



^1H NMR (300 MHz, CDCl_3) δ 7.50 (s, 1H, H5), 7.44 (s, 1H, H2), 7.27 (d, $J=12.4$ Hz, 2H, H1 and H3), 3.11 (s, 1H, H8), 2.85 (m, 2H, H10 and H12), 2.75 (m, 2H, H10 and H12), 2.11 (m, 2H, H9 and H13), 1.90 (m, 2H, H9 and H13). ^{13}C NMR (75 MHz, CDCl_3) δ 140.0 (C4), 135.9 (C6),

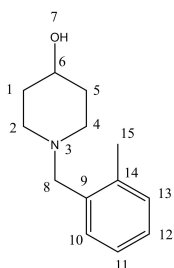
130.0 (C3), 129.9 (C1), 126.2 (C2), 125.2 (C5), 124.1 (C14), 72.9 (C7), 44.1 (C10 and C12), 37.8 (C9 and C13). $M/Z = 245.10$ g/mol. Light brown oil. Yield = 53 %

FMD-0



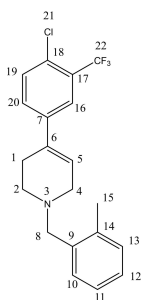
^1H NMR (300 MHz, CDCl_3) δ 7.50 (s, 6H), 7.29 (s, 2H), 7.24 (d, $J = 38.3$ Hz, 10H), 2.88–2.81 (m, 12H), 2.78–2.71 (m, 12H), 2.35 (s, 6H), 2.12–2.08 (m, 9H), 1.92–1.86 (m, 11H), 1.71 (s, 6H). ^{13}C NMR (75 MHz, CDCl_3) δ 139.1 (C4), 136.1 (C6), 134.2 (C2), 131.3 (C3), 129.7 (C1), 124.4 (C5), 124.0 (C15), 72.9 (C7), 44.1 (C10 and C12), 37.8 (C9 and C13). $M/Z = 279.06$ g/mol. Brown oil. Yield = 25 %

FMD-16



^1H NMR (300 MHz, CDCl_3) δ 7.22 (s, 1H, H10), 7.16 (m, 3H, H11, H12 and H13), 3.67 (s, 2H, H8), 3.61 (m, 1H, H6), 2.65 (m, 2H, H2 and H4), 2.35 (s, 3H, H15), 2.31 (m, 2H, H2 and H4), 1.94 (m, 2H, H1 and H5), 1.75 (m, 2H, H1 and H5). ^{13}C NMR (75 MHz, CDCl_3) δ 138.1 (C9), 136.5 (C14), 130.3 (C13), 128.1 (C10), 126.6 (C11), 125.3 (C12), 65.6 (C6), 61.6 (C8), 51.1 (C2 and C4), 34.5 (C1 and C5), 19.4 (C15). $M/Z = 205.15$ g/mol. Yellow oil. Yield = 74 %

FMD-37



^1H NMR (300 MHz, CDCl_3) δ 7.50 (s, 1H), 7.23 (d, $J = 1.1$ Hz, 2H, H19 and H20), 7.18 (m, 2H, H10 and H11), 7.15 (m, 1H, H12), 7.12 (m, 1H, H13), 6.31 (s, 1H, H5), 4.07 (s, 1H, H8), 3.56 (m, 2H, H4), 3.18 (s, 1H, H8), 2.80 (s, 1H, H2), 2.56 (s, 1H, H2), 2.51 (m, 2H, H1), 2.33 (m, 3H, H15). ^{13}C NMR (75 MHz, CDCl_3) δ 140.7 (C7), 138.1 (C9), 136.5 (C14), 132.3 (C17), 132.3 (C20), 130.9 (C19), 130.8 (C6), 130.4 (C18), 130.3 (C13), 128.1 (C10), 126.6 (C11), 125.3 (C12), 124.4 (C16), 124.0 (C22), 119.2 (C5), 60.0 (C8), 52.3 (C4), 51.2 (C2), 28.7 (C1), 19.4 (C15). $M/Z = 365.12$ g/mol. Brown oil. Yield = 19 %

Biology

Cytotoxicity assay. Cell viability was determined using Vero epithelial cells which were grown in RPMI medium containing 10% fetal bovine serum (RPMI-FBS) and differentiated with 20 ng/ml phorbol myristate acetate (PMA) and incubated for 48 h at 37 °C, under a 5% CO_2 atmosphere. Cells were seeded in 96-well plates at a density of 2×10^4 cells/well in 160 μl medium and incubated overnight at 37 °C to allow cells to adhere. Compounds (dissolved in DMSO) were freshly diluted in RPMI starting at a concentration of 100 $\mu\text{g}/\text{ml}$ up to a concentration of 0.048 $\mu\text{g}/\text{ml}$ (serial dilution of factor 2), and 20 μl of those dilution were added in corresponding wells. The maximum final concentration of DMSO was 1% (v/v). After 24 h incubation at 37 °C with 5% CO_2 , 20 μl of 1 mg/ml resazurin (Sigma, Germany) was added to each well and the cells incubated for an additional 2 hours at 37 °C in the presence of 5% CO_2 . Fluorescence was then measured in a Polarstar Omega fluorometer using appropriate filters (590 nm emission and 540 nm excitation wavelength). Percentage survival was determined by dividing fluorescence values obtained in the compound containing wells by values obtained for control wells containing cells incubated with a dilution series of DMSO (serial dilution of factor 2 from 1% to 0.000488% v/v). Experiments were complete in triplicate on three independent events.

Drug susceptibility testing. To determine the MICs, broth micro-dilution method in CaMHB using an inoculum containing 5×10 CFU/ml in the exponential-growth phase were achieved following the CLSI guidelines.^[28] Briefly, 100 μl of bacteria were seeded in 96-well plates, and 2 μl of drug at its highest concentration in a maximum of 1% of DMSO (v/v) was added to the first wells containing 200 μl of bacterial suspension and a twofold serial dilutions were then done out. Incubation with drugs was performed at 30 °C for 3 to 5 days. MICs were recorded by visual inspection and by absorbance at 560 nm to confirm visual recording. Experiments were done in triplicate on three independent occasions.

Molecular Modelling

Comparative modelling of MAB_4508 was performed using Modeller^[35] and the crystal structure (2.8 Å, PDB ID: 6AJJ) of a mycolic acid transporter from *M. smegmatis* (Sequence identity: 64.9%) as template. Quality of the model was assessed using MolProbity.^[36] Subsequent energy minimization of the global model was performed using AMBER forcefield in order to remove putative steric clashes between side chains. Simulation of the binding modes of the target and the designed compounds was performed using GOLD docking program.^[37] GOLD is based on a genetic algorithm and considered the ligand as flexible, while side chains of most residues are kept rigid. For the search procedure, a sphere of 10 Å was centred on the X, Y and Z coordinates of our identified binding centre. Then, all the different binding poses were scored with the ChemPLP scoring function. Subsequent energy minimization was performed using the AMBER forcefield. Finally, all the molecular representations were sketched using PyMOL.^[38]

Toxicologic and Pharmacokinetics Studies; Mouse Blood and Tissue Sampling

Experimental compound PIPD1 was administered either intraperitoneally, intravenously or by oral gavage. For toxicologic studies, PIPD1 was diluted in DMSO at different concentrations in order that mice receive either intraperitoneally or intravenously the doses of 250 mg/kg, 100 mg/kg, 50 mg/kg and 10 mg/kg in a total volume of 50 μl corresponding respectively to 5 mg, 2, 1 and 0.2 mg/mice. Control groups were administered with the equivalent volume of

DMSO alone. Groups were constituted of $n=3$ mice. Mice were observed during 4 days. For pharmacokinetic studies, the chosen concentration was 50 mg/kg, i.e. 1 mg/mice for intraperitoneally administration. 100 μ l of blood was taken from the retro-orbital plexus at different time points (5 min, 1 h, 3 h, 5 h, 6 h, 8 h, 12 h, 18 and 24 h), sera were separated after 1 h at 37 °C for red cells coagulation using centrifugation at 10,000 g during 10 min and were stored at -30 °C until analysis. Organs (spleen, lungs, liver, heart, kidneys and brain) were collected at the last time point when mice were sacrificed. Experiment was repeated two times with $n=7$ mice. For administration by oral gavage, mice ($n=3$) received the same quantity of PIPD1, 1 mg/mice, diluted in a total volume of 200 μ l of glycerol. The time of organ collection were 4 h, 5 h and 24 h and sera collection were 1 h, 2 h, 3 h, 4 h, 5 h and 24 h.

All procedures were applied according to the ethics guidelines (Approval number APAFIS#11465-201611417574906 from the ethics committee A783223)

Concentrations of PIPD1 in organs and collected sera were analysed by liquid chromatography/mass spectrometry (LC/MS) as described below.

Quantification of PIPD1 in Murine Tissues and Fluids

Samples were processed using liquid-liquid extraction and PIPD1 was quantified with liquid chromatography coupled to mass spectrometry. Briefly, ten microliters of the internal standard working solution (penfluridol 10 μ g/mL) and 1 ml of the extracting solvent (tert-butyl methyl ether/hexane, 50/50 (v/v)) were added to each tube containing either about 50 mg of tissue or 50 μ l of plasma. Solid tissue samples were crushed and homogenized using a ball mill TissueLyser LT (Qiagen, Courtaboeuf, France) and a 5 mm stainless steel bead for 20 min with an oscillation frequency of 50 Hz whereas cell culture supernatant samples were shaken for 10 min with an RM-2L Intelli-mixer (Elmi, Riga, Latvia). Tubes were then centrifuged at 13,300 rpm for 10 min. The upper organic layer was decanted into another tube and evaporated to complete dryness under vacuum at 43 °C. Samples were reconstituted with 80 μ l of 0.1% formic acid/LC-MS methanol (30:70, v/v), then vortex mixed for 30 s, and transferred into injection vials for analysis.

Chromatography was performed with an UltiMate 3000 Quaternary Rapid Separation Pump LPG-3400RS (Thermo Scientific Dionex, Les Ulis, France), using a 1.9 μ m C18 Hypersil Gold column (100 \times 2.1 mm i.d.) (ThermoFisher) maintained at 30 °C. 10 μ l were injected in the chromatographic system. Elution was achieved in the isocratic mode with the following mobile phase composition: 30% of aqueous buffer (0.1% formic acid) and 70% of methanol. The flow rate was 200 μ l/min at the start and until 1.8 min, then changed to 300 μ l/min until 4 min, after what it returned to 200 μ l/min. Total run time was 5.0 min.

Compounds were detected with a triple quadrupole Quantiva mass spectrometer (ThermoFisher) equipped with a heated electrospray ionization source. Nitrogen (N2-45 nitrogen generator, VWR International, Fontenay sous bois, France) was employed as sheath and auxiliary gas. The HESI source was set in positive ionization with the following parameters: sheath gas flow rate: 45; aux. gas flow rate: 10; sweep gas: 1; spray voltage: 2.4 kV; ion transfer tube temp.: 300 °C; vaporizer temp.: 100 °C. Data acquisition was performed in the multiple reaction monitoring mode with the following ions (m/z) monitored for each compound were (parent ion \rightarrow product ion (collision energy (V))): PIPD1: 384.3 \rightarrow 105.4 (26); 384.3 \rightarrow 261.9 (19) and 384.3 \rightarrow 278.0 (20); penfluridol (IS): 524.1 \rightarrow 183.0 (55) and 524.1 \rightarrow 291.9 (36) and their retention times were 2.2 and 4.2 min, respectively. Chromatographic data acquisition and processing

were performed using the Chromeleon v6.80 (Thermo Scientific Dionex) and Xcalibur v3.0.63 (ThermoFisher) softwares.

A calibration curve including a zero and seven calibration standards was performed with each series of experiments. Quantitation was achieved by plotting the peak area ratios of PIPD1 to the internal standard versus concentration followed by mean least squares linear regression. A 1/x weighing factor was applied to the linear regression to correct for data heteroscedasticity. The lower limit of quantification (LLOQ) was 0.1 ng/ml for plasma samples and 0.1 pg/mg for tissue samples, the upper limit of quantification (ULOQ) was 5000 ng/mL and 5000 pg/mg, respectively. Data for tissue analysis are expressed as ng/ μ g of tissue; for plasma as ng/ml.

Pharmacokinetic Modelling

Data was analysed using the nonlinear mixed effect modelling software program Monolix v4.4.0 (Lixoft, Orsay, France).^[34] A two-compartment open model was fitted and the parameters were estimated by computing the maximum likelihood estimator of the parameters without any approximation of the model (no linearization) using the stochastic approximation expectation maximization algorithm combined to a Markov Chain Monte Carlo procedure.

Acknowledgements

This work was supported by the French National Research Agency MyCat Grant ANR-15-CE18-0007-02 (to L. K. and Y. G.).

Conflict of Interest

The authors declare no conflict of interest.

Keywords: *mycobacterium abscessus* · molecular modeling · structure-activity relationship · phenotypic screening · piperidinol derivatives

- [1] J. R. Honda, R. Viridi, E. D. Chan, *Front. Microbiol.* **2018**, *9*, 2029.
- [2] T. A. Claeys, R. T. Robinson, *J. Bacteriol.* **2018**, *200*, e00739-17.
- [3] Y. Nishiuchi, T. Iwamoto, F. Maruyama, *Frontiers in Medicine* **2017**, *4*, DOI 10.3389/fmed.2017.00027.
- [4] E. Tortoli, *Clin. Microbiol. Rev.* **2014**, *27*, 727–752.
- [5] J. van Ingen, *Semin. Respir Crit Care Med* **2013**, *34*, 103–109.
- [6] P. M. Cassidy, K. Hedberg, A. Saulson, E. McNelly, K. L. Winthrop, *Clin. Infect. Dis.* **2009**, *49*, e124–129.
- [7] M. J. Donohue, *BMC Infect. Dis.* **2018**, *18*, 163.
- [8] V. Litvinov, M. Makarova, K. Galkina, E. Khachatourians, M. Krasnova, L. Guntupova, S. Safonova, *PLoS One* **2018**, *13*, e0203108.
- [9] K. Ryan, T. F. Byrd, *Front. Microbiol.* **2018**, *9*, 2642.
- [10] J. M. Bryant, D. M. Grogono, D. Rodriguez-Rincon, I. Everall, K. P. Brown, P. Moreno, D. Verma, E. Hill, J. Drijkoningen, P. Gilligan, *Science* **2016**, *354*, 751–757.
- [11] D. E. Griffith, T. Aksamit, B. A. Brown-Elliott, A. Catanzaro, C. Daley, F. Gordin, S. M. Holland, R. Horsburgh, G. Huitt, M. F. Iademarco, *Am. J. Respir. Crit. Care Med.* **2007**, *175*, 367–416.
- [12] R. A. Floto, K. N. Olivier, L. Saiman, C. L. Daley, J.-L. Herrmann, J. A. Nick, P. G. Noone, D. Bilton, P. Corris, R. L. Gibson, *Thorax* **2016**, *71*, 88–90.
- [13] S. L. Martiniano, M. K. Sontag, C. L. Daley, J. A. Nick, S. D. Sagel, *Ann Am Thorac Soc* **2014**, *11*, 36–44.
- [14] T. Qvist, D. Taylor-Robinson, E. Waldmann, H. V. Olesen, C. R. Hansen, I. H. Mathiesen, N. Høiby, T. L. Katzenstein, R. L. Smyth, P. J. Diggle, *J. Cyst. Fibros.* **2016**, *15*, 380–385.
- [15] D. E. Griffith, *F1000Prime Rep* **2014**, *6*, 107.

- [16] R. M. Doyle, M. Rubio, G. Dixon, J. Hartley, N. Klein, P. Coll, K. A. Harris, *Clin. Infect. Dis.* **2019**, DOI 10.1093/cid/ciz526.
- [17] J. E. Gross, S. L. Martiniano, J. A. Nick, *Curr. Opin. Pulm Med* **2019**, *25*, 646–653.
- [18] K. C. Malcolm, S. M. Caceres, J. R. Honda, R. M. Davidson, L. E. Epperson, M. Strong, E. D. Chan, J. A. Nick, *Appl. Environ. Microbiol.* **2017**, *83*, DOI 10.1128/AEM.00562-17.
- [19] B. A. Brown-Elliott, S. Vasireddy, R. Vasireddy, E. Iakhsiaeva, S. T. Howard, K. Nash, N. Parodi, A. Strong, M. Gee, T. Smith, *J. Clin. Microbiol.* **2015**, *53*, 1211–1215.
- [20] B. A. Brown-Elliott, K. A. Nash, R. J. Wallace, *Clin. Microbiol. Rev.* **2012**, *25*, 545–582.
- [21] J. Chen, L. Zhao, Y. Mao, M. Ye, Q. Guo, Y. Zhang, L. Xu, Z. Zhang, B. Li, H. Chu, *Front. Microbiol.* **2019**, *10*, 1977.
- [22] M. Lu, D. Fitzgerald, J. Karpelowsky, H. Selvadurai, C. Pandit, P. Robinson, B. J. Marais, *Breathe (Sheff)* **2018**, *14*, 288–301.
- [23] A. Tissot, M. F. Thomas, P. A. Corris, M. Brodli, *BMC Pulm. Med.* **2018**, *18*, DOI 10.1186/s12890-018-0635-3.
- [24] D. Raats, N. Lorent, V. Saegeman, R. Vos, J. Van Ingen, G. Verleden, D. Van Raemdonck, L. Dupont, *Transpl Infect Dis* **2018**, e13046.
- [25] L. Ballell, R. H. Bates, R. J. Young, D. Alvarez-Gomez, E. Alvarez-Ruiz, V. Barroso, D. Blanco, B. Crespo, J. Escribano, R. González, *ChemMedChem* **2013**, *8*, 313–321.
- [26] C. Dupont, A. Viljoen, F. Dubar, M. Blaise, A. Bernut, A. Pawlik, C. Bouchier, R. Brosch, Y. Guérardel, J. Lelièvre, *Mol. Microbiol.* **2016**, *101*, 515–529.
- [27] A. E. Grzegorzewicz, H. Pham, V. A. K. B. Gundi, M. S. Scherman, E. J. North, T. Hess, V. Jones, V. Gruppo, S. E. M. Born, J. Korduláková, *Nat Chem Biol* **2012**, *8*, 334–341.
- [28] C. Varela, D. Rittmann, A. Singh, K. Krumbach, K. Bhatt, L. Eggeling, G. S. Besra, A. Bhatt, *Chem. Biol.* **2012**, *19*, 498–506.
- [29] G. Degiacomi, A. Benjak, J. Madacki, F. Boldrin, R. Proveddi, G. Palù, J. Kordulakova, S. T. Cole, R. Manganelli, *Sci. Rep.* **2017**, *7*, 43495.
- [30] A. Viljoen, V. Dubois, F. Girard-Misguich, M. Blaise, J.-L. Herrmann, L. Kremer, *Mol. Microbiol.* **2017**, *104*, 889–904.
- [31] C. Dupont, Y. Chen, Z. Xu, F. Roquet-Banères, M. Blaise, A.-K. Witt, F. Dubar, C. Biot, Y. Guérardel, F. P. Maurer, *J. Biol. Chem.* **2019**, DOI 10.1074/jbc.RA119.010135.
- [32] G. L. Woods, B. A. Brown-Elliott, P. S. Conville, E. P. Desmond, G. S. Hall, G. Lin, G. E. Pfyffer, J. C. Ridderhof, S. H. Siddiqi, R. J. Wallace, *Susceptibility Testing of Mycobacteria, Nocardiae, and Other Aerobic Actinomycetes*, Clinical And Laboratory Standards Institute, Wayne (PA), **2011**.
- [33] B. Zhang, J. Li, X. Yang, L. Wu, J. Zhang, Y. Yang, Y. Zhao, L. Zhang, X. Yang, X. Yang, *Cell* **2019**, *176*, 636–648.e13.
- [34] E. Kuhn, M. Lavielle, *Computational Statistics & Data Analysis* **2005**, *49*, 1020–1038; *Data Analysis* **2005**, *49*, 1020–1038.
- [35] A. Sali, T. L. Blundell, *J. Mol. Biol.* **1993**, *234*, 779–815.
- [36] C. J. Williams, *Protein Sci.* **2018**, *27*, 293–315.
- [37] G. Jones, P. Willett, R. C. Glen, A. R. Leach, R. Taylor, *J. Mol. Biol.* **1997**, *267*, 727–748.
- [38] W. L. DeLano, 2002, The PyMOL Molecular Graphics System. Delano Scientific, San Carlos.

Manuscript received: February 14, 2020